Ribonuclease Sa Conformational Stability Studied by NMR-Monitored Hydrogen Exchange†

Douglas V. Laurents,‡ J. Martin Scholtz,§ Manuel Rico,‡ C. Nick Pace,*,§ and Marta Bruix*,‡

Instituto de Química Física "Rocasolano", CSIC, Serrano 119, Madrid 28006, Spain, and Department of Medical Biochemistry and Genetics, Texas A&M University College of Medicine, 440 Reynolds Medical Building, College Station, Texas 77843

Received January 25, 2005; Revised Manuscript Received April 5, 2005

ABSTRACT: The conformational stability of ribonuclease Sa (RNase Sa) has been measured at the per-residue level by NMR-monitored hydrogen exchange at pH* 5.5 and 30 °C. In these conditions, the exchange mechanism was found to be EXII. The conformational stability calculated from the slowest exchanging amide groups was found to be 8.8 kcal/mol, in close agreement with values determined by spectroscopic methods. RNase Sa is curiously rich in acidic residues (pI = 3.5) with most basic residues being concentrated in the active-site cleft. The effects of dissolved salts on the stability of RNase Sa was studied by thermal denaturation experiments in NaCl and GdmCl and by comparing hydrogen exchange rates in 0.25 M NaCl to water. The protein was found to be stabilized by salt, with the magnitude of the stabilization being influenced by the solvent exposure and local charge environment at individual amide groups. Amide hydrogen exchange was also measured in 0.25, 0.50, 0.75, and 1.00 M GdmCl to characterize the unfolding events that permit exchange. In contrast to other microbial ribonucleases studied to date, the most protected, globally exchanging amides in RNase Sa lie not chiefly in the central β strands but in the 3/10 helix and an exterior β strand. These structural elements are near the Cys7−Cys96 disulfide bond.

Ribonuclease Sa (RNase Sa) is a very small (96-residue) enzyme secreted by *Streptomyces aureofaciens*. RNase Sa shares the same basic $\alpha + \beta$ fold (*1*, *2*) observed in other microbial ribonucleases such as RNases T1 (3), Ba (barnase) (*4*), and α-sarcin (*5*). The secondary structure is composed of a two-stranded β-sheet formed by residues 5−7 and 91−93, a turn of 3/10 helix (residues 8−11), followed by an α-helix, residues 15−23, and a four-stranded antiparallel β-sheet, residues 35−36, 52−54, 70−73, and 80−81. RNase Sa contains six prolines, five of which form trans peptide bonds, with the lone exception of the cis Gly26−Pro27 linkage. Asn39 in RNase Sa is conserved among microbial ribonuclease and forms three hydrogen bonds, which make important contributions to the stability of RNase Sa (*6*). The active site is found on the concave face of the sheet, while the α-helix packs against the opposite, convex side (Figure 1A). RNase Sa and its homologues and variants have proven to be useful models for studying protein activity and solubility (*7*), electrostatics in the native (*8*, *9*) and unfolded states (*10*), and conformational stability (*11*, *12*).

In comparison to other ribonucleases, RNase Sa is remarkably rich in acidic residues; its surface is dominated by negative charges near neutral pH (Asp + Glu + C terminus = 13, Arg + His + Lys + N terminus = 8). This is peculiar because the job of this enzyme is to bind and cleave RNA, a large negatively charged substrate. The positive charged residues are concentrated on the side of the protein with the active site, presumably to help attract the substrate, whereas the negative-charged residues are abundant on the other face (Figure 1B). This segregation of oppositely charged groups might aid the protein to function, but it concentrates like charges, which should produce electrostatic repulsion and destabilize the protein. In fact, the p*K* values of titratable groups in RNase Sa are strongly influenced by charge−charge interactions (*8*, *9*, *12*), and the protein is stabilized in the presence of 0.5 M NaCl (*11*). Understanding how salt affects the stability of RNase Sa and other proteins is difficult because the action of salt is complex; it could act by binding tightly to specific sites on the protein, by screening electrostatic interactions, or both. Moreover, the energetic effects of electrostatic screening have important effects on the stability of the native state as well as on the stability and distribution of structures in the denatured state ensemble (*10*, *13*).

Here, we decided to further study the electrostatic interactions in RNase Sa by two methods. First, thermal unfolding experiments were performed to measure the stability of RNase Sa in various concentrations of NaCl and guanidinium chloride (GdmCl).[1] These studies use high temperatures to provoke unfolding, requiring extrapolation to physiological conditions to determine the free energy of the global unfolding transition (ΔG_U). In contrast, hydrogen exchange

† This work was supported by the Dirección General de Investigación Científica y Técnica (Spain) (PB-93-0189 to M.R.), by the NIH (GM 37039 to C.N.P. and GM 52483 to J.M.S.), and the Robert A. Welch Foundation (BE-1060 to C.N.P. and BE-1281 to J.M.S.). D.V.L. was supported by fellowships from the Leukemia and Lymphoma Society and the Ramón y Cajal program (Spain).

* To whom correspondence should be addressed. Telephone: +34-91-561-9400 (ext 1455). Fax: +34-91-564-2431. E-mail: mbruix@iqfr.csic.es (M.B.); Telephone: 979-845-1788. Fax: 979-847-9481. E-mail: nickpace@tamu.edu (C.N.P.).

‡ CSIC.

§ Texas A&M University College of Medicine.

10.1021/bi050142b CCC: $30.25
Published on Web 05/06/2005

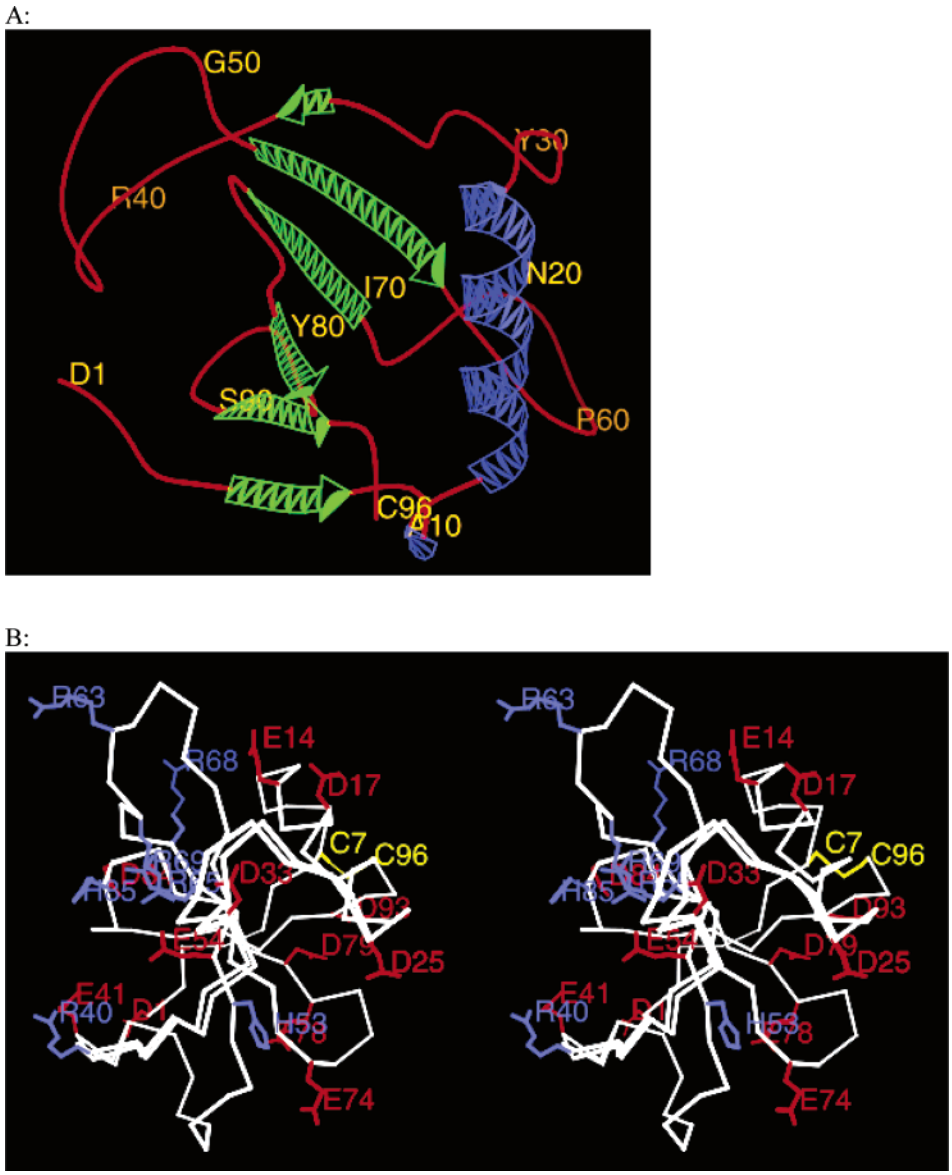

FIGURE 1: RNase Sa structure. (A) Secondary structure, ribbon diagram showing helices in blue, β strands in green, and other regions in red. The N- and C-terminal residues and every 10th residue are labeled. (B) Segregation of charges. Stereopair of the RNase Sa structure (PDB 1LNI) showing positively charged side chains in blue, negatively charged side chains in red, and the Cys7−Cys96 disulfide bond in yellow.

measurements are typically made under near physiological conditions and give per-residue information on the conformational stability (ΔG_{HX}). In general, many amide protons are found to exchange from partially unfolded states, whereas others only exchange upon complete unfolding. The ΔG_{HX} values from the latter group of residues typically agree with the ΔG_U values from conventional measurements, once the contributions of proline isomerization and the influences of the solvent (H_2O versus D_2O) are taken into account (*14*). Therefore, as a second approach toward studying the effect of salt on RNase Sa stability, the hydrogen exchange rates are measured for individual amide groups in D_2O alone or with 0.25 M NaCl or 0.25 M GdmCl and compared to rates from unstructured peptides (*15*, *16*).

Early qualitative results found slow exchanging residues in the 3/10 helix and C-terminal β strand of RNase Sa in addition to the central β-sheet (*17*). This is rather surprising because, in other homologous, well-studied microbial ribonucleases, RNases T1 and Ba (barnase), and α-sarcin, the slowest exchanging residues are in the central β-sheet. To investigate this result further, we have now measured the hydrogen exchange rate constants for native RNase Sa in four different concentrations of GdmCl. These measurements aim to reveal the magnitude of the unfolding events that permit exchange at individual residues, because the *m* value (the dependence of the local conformation stability measured by hydrogen exchange) has been shown to be proportional to the size of the unfolding event (*18*, *19*).

EXPERIMENTAL PROCEDURES

Protein Samples. RNase Sa (recombinant) was expressed in *Escherichia coli* (strain RY 1988) containing the expression plasmid pEH100. RNase Sa was uniformly labeled with ^{15}N by growing cells in M9 minimal media to 1.2−1.5 OD,

[1] Abbreviations: CD, circular dichroism; GdmCl, guanidinium chloride; ΔG_{HX}, hydrogen exchange stability; $\Delta G_U(D_2O)$, stability in 0 M denaturant measured in D_2O; $\Delta G_U(H_2O)$, stability in 0 M denaturant measured in H_2O; H-bond, hydrogen bond; k_{rc}, intrinsic chemical exchange rate constant; NH, amide proton; pH*, the pH meter reading in D_2O without correction for the deuterium isotope effect.

collecting the cells by centrifugation, and then resuspending them in media containing $^{15}NH_4Cl$ as the source of ^{15}N, with 0.1 mM IPTG to induce protein production. RNase Sa was purified as described by Hebert et al. (*20*), and the yield was 20−25 mg/L. NMR samples contained about 2 mM RNase Sa and were dissolved in 0.5 mL of D_2O (>99.9% atom D) (Apollo Sci. Ltd., Derbyshire, U.K.). TSP was used as the internal chemical-shift standard. GdmCl was "ultra pure" grade from ICN Biomedicals, Inc. (Aurora, OH), and the NaCl was from D'Hemio Laboratorios (Madrid, Spain).

Amide Protein Hydrogen Exchange Theory. When a protein is put in D_2O, its amide protons begin to exchange with solvent deuterons. This process can be modeled as a two-step reaction, wherein a closed conformation first opens, which then permits exchange with a rate constant, k_{rc}, which depends on temperature, pH, and the neighboring side chains (*15*, *16*)

$$(B-H\cdots A) \underset{k_{cl}}{\overset{k_{op}}{\rightleftharpoons}} (B-H)\,(A) \xrightarrow{k_{rc}} B-D \qquad (1)$$

In this formula, k_{op} is the rate constant for the opening or unfolding reaction, k_{cl} is the rate constant for the closing or folding reaction, and k_{rc} is the intrinsic exchange rate constant. When the closed form is strongly favored such that $k_{cl} \gg k_{op}$, the observed exchange rate constant, k_{obs}, is given by (*21*)

$$k_{obs} = \frac{k_{op}k_{rc}}{k_{cl} + k_{rc}} \qquad (2)$$

In the limiting case where k_{rc} dominates k_{cl} and therefore also k_{op}, this equation further simplifies to

$$k_{obs} = k_{op} \qquad (3)$$

This limiting case is known as EXI and is sometimes observed at high pH where k_{rc} is very large and can be exploited to measure per-residue unfolding rates in proteins (*22*). When, in turn, the closing reaction rate constant k_{cl} is larger than the exchange k_{rc} (ie., $k_{cl} \gg k_{rc}$), eq 2 simplifies to

$$k_{obs} = \frac{k_{op}k_{rc}}{k_{cl}} \text{ or } K_{op}k_{rc} \qquad (4)$$

where K_{op} is the equilibrium constant of the opening reaction. This limiting case, called EXII, is frequently observed for proteins, particular below pH 7. From K_{op}, the free energy of the opening/closing or folding/denaturing equilibrium, ΔG_{HX}, can be calculated using the Gibbs equation

$$\Delta G_{HX} = -RT \ln K_{op} \qquad (5)$$

where R is the gas constant and T is the absolute temperature. Because the EXI exchange mechanism is OH^--independent and EXII is not (*21*), it is possible to determine which dominates by measuring exchange at different pH.

The sensitivity of the free energy to the denaturant concentration corresponds to the amount of apolar surface area exposed by the unfolding event (*23*). Therefore, the size of the local unfolding events that permit the exchange of a particular residue "*i*" can be determined from the slope of the dependence of $\Delta G_{HX(i)}$ on the denaturant concentration (*18*, *19*), using the linear equation

$$\Delta G_{HX(i)}(\text{Den}) = m_i[\text{Den}] + \Delta G_{HX(i)}(D_2O) \qquad (6)$$

where $\Delta G_{HX(i)}$(Den) is the free energy of *i* at a particular concentration of GdmCl, [Den] is the denaturant concentration, $\Delta G_{HX}(D_2O)$ is the free energy in D_2O, and the slope, m_i, measures the size of the unfolding event around residue "*i*". While the effect of GdmCl on the amide group hydrogen exchange from most amino acid residues is unknown, GdmCl was shown to produce a slight increase (20% at 1 M) in the k_{rc} for poly-(D,L)-alanine (*24*). The results reported here do not include this small apparent decrease of 0.1 kcal/mol in the stability measured by hydrogen exchange in GdmCl that results from this slightly larger k_{rc} rate constant.

Hydrogen Exchange by NMR Spectroscopy. The exchange of amide protons with solvent deuterons was started by dissolving lyophilized, protonated ^{15}N-RNase Sa into deuterated solvent. A summary of the data collection is given in the Supplementary Table 1 in the Supporting Information. The temperature was 30 °C, and the pH* of the exchange experiments was pH* 5.5, except for experiments done at pH* 6.0 and 7.0 to determine the exchange mechanism. pH* 5.5 was chosen because it is high enough so that exchange will be fast enough to permit the measurement of even the slowest exchanging groups but low enough so that exchange will proceed by the EXII mechanism. The hydrogen exchange rates were determined by integrating the volume of ^1H-^{15}N amide cross-peaks in a series of HSQC spectra (*25*). The peak volume versus time data were fit to a single-exponential decay function equation using a least-squares algorithm to yield the exchange rate. Equations 4, 5, and 6 given above and the values of k_{rc} measured in short peptides and corrected to pH* 5.5 and 30 °C as described previously (*16*) were used to calculate protection factors and values of ΔG_{HX} and m_i from the exchange rates.

Denaturation Experiments. The conformational stability of RNase Sa in H_2O (pH 5.9) or D_2O (pH* 5.5) at 30 °C was determined by GdmCl denaturation monitored by circular dichroism (CD) at 234 nm using a Jasco CD spectrometer equipped with a Peltier temperature control unit in a 0.5 cm cell. The denaturation in D_2O was performed using initially protonated RNase Sa, which gained deuterium during the unfolding, as occurs during hydrogen exchange (*26*). The data were analyzed by fitting to a least-squares algorithm (*27*) as previously described (*28*). The contribution of proline isomerization, which reaches equilibrium in the GdmCl denaturated state but not the transiently unfolded states that permit hydrogen exchange was calculated for the five trans Pro and one cis Pro bond in folded RNase Sa using the cis/trans ratio for X−Pro bonds determined in short peptides by Fischer and co-workers (*29*) and found to be 1.60 kcal/mol at 30 °C.

The stability of unlabeled RNase Sa, approximately 0.4 mM, in varying concentrations of NaCl or GdmCl, was determined by thermal denaturation. Except for one sample, which contained no salt or buffer, 50 mM sodium acetate was used to maintain the pH at 5.9. The reversibility of the experiments was checked by recooling the sample after thermal unfolding, measuring the CD signal of the renatured sample, and was found to be better than 98%. A two-state

unfolding model was fit to the data using a least-squares algorithm to obtain ΔH, the enthalpy change for folding, T_m, the midpoint of the thermal transition, and ΔS, the entropy change for folding. Changes in the stability were calculated using the approximation $\Delta(\Delta G) \approx \Delta S \Delta T_m$ (*30*).

Structure Analysis. Structure figures were prepared using PREKIN and MAGE (Prof. David C. Richardson, Little River Institute, Durham, NC) using coordinates from the atomic resolution structure (1.0 Å) (PDB 1LNI) of RNase Sa (*31*). The exposed surface area (probe depth radius = 1.4 Å) and hydrophobic contacts (cutoff distance = 4 Å) were determined using MolMol (*32*) and the structures of RNase Sa (*31*), RNase T1 (33), RNase Ba (*34*), and α-sarcin (*5*).

RESULTS

The Exchange Mechanism of RNase Sa at pH 5.5 and 30 °C Is EXII.* The rate of hydrogen exchange reflects (i) the unfolding rate of individual amide groups, i.e., EXI exchange, (ii) the equilibrium between the folded and unfolded states of individual amide groups, i.e., EXII exchange, or (iii) a combination of these two limiting cases (*21*). Because EXII exchange is base-catalyzed above pH ≈4, while EXI exchange is pH-independent, the nature of the exchange mechanism can be determined by monitoring hydrogen exchange at different pH values (*21*). For RNase Sa, exchange was measured at pH* 5.5, 6.0, and 7.0. The exchange of two typical protons is shown in Figure 2A, and the exchange rates are compared in Figure 2B. Between pH* 5.5 and 6.0, there is a linear correspondence between the logarithm of the exchange rates whose slope is, within error, 1.0 (Figure 2B); this indicates that EXII is the dominant exchange mechanism within this pH* range (*35*). This conclusion is corroborated by the observation that many residues with similar ΔG_{HX} values have quite different k_{rc} values (see Table 1 and ref *14*). Equations 4 and 5 can be used to determine the local conformational stability at each NH from the exchange rate constants at pH* 5.5. The slope of the exchange rate constants measured at pH* 5.5 versus 7.0 is, in contrast, reduced to about 0.5 (Figure 2B), indicating that exchange proceeds by a mixture of the EXI and EXII mechanisms at pH 7.0.

The Slowest Exchanging Amide Protons Are Near the Disulfide Bond. The rate constants for the hydrogen exchange of RNase Sa at pH* 5.5 and 30 °C in D_2O are given in Table 1, and the corresponding protection factors and conformational free energies are shown in Figure 3. The uncertainties in the exchange rates varied from ±5% in favorable cases to ±15% for less favorable cases, where amide protons exchanged relatively fast or slow relative to the acquisition of NMR spectra. Because of the logarithmic dependence of the conformational free energies on the exchange rates, these uncertainties propagate to relatively small values in the free energies, ΔG_{HX}; the average error was 0.9% with a standard deviation of 1.4%. The exchange experiment in D_2O was repeated once. The rates were found to agree within 30%, and the corresponding ΔG_{HX} values vary by 0.16 kcal/mol on average (data not shown). Amide protons with rate constants greater than ≈2 h^{-1} exchanged in the dead time of the NMR spectral acquisition and thus define the lower limit for protection factors of 400−3000, depending on the

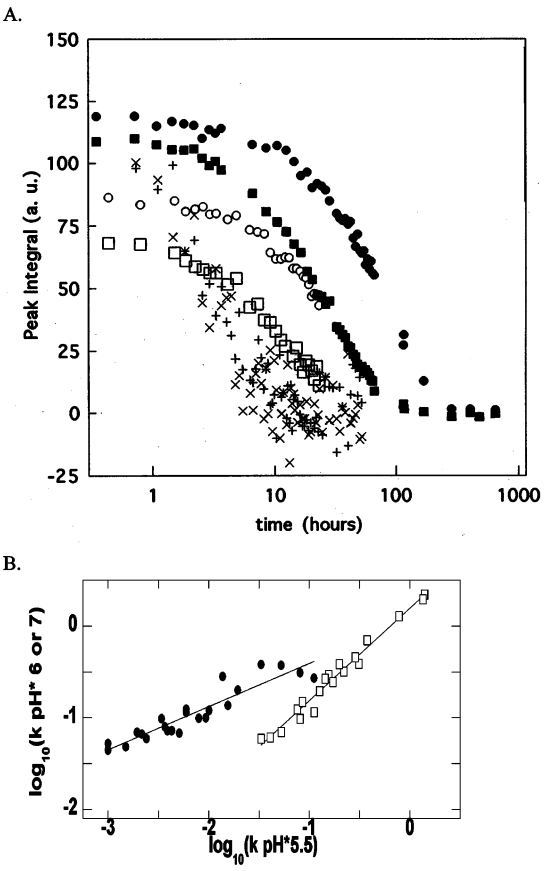

FIGURE 2: pH* dependence of hydrogen exchange in RNase Sa. (A) Hydrogen exchange behavior of amide protons in RNase Sa at pH* 5.5, 6.0, and 7.0 is shown. pH* 5.5: Asn20, ●; Cys96, ■. pH* 6.0: Asn20, ○; Cys96, □. pH* 7.0: Asn 20, +; Cys96, ×. (B) Variation in the exchange rates for amide groups at pH* 5.5 versus 6.0 (□) or 7.0 (●) is shown. The lines represent the least-squares fit of a linear equation to the data. Many of the amide groups compared for pH* 5.5 versus pH* 6.0 are different than those compared for pH* 5.5 versus pH* 7.0 (see Table 1).

side chains neighboring the amide group. Several residues, Val36, Tyr52, Ile58, Thr59, and Asp79, show slowed exchange but do not appear to form intramolecular hydrogen bonds according to the analysis of the 1.0 Å crystal structure of RNase Sa (*31*). The slowed exchange of these amide groups seems to be due to hydrogen bonding to structural water molecules, burial, or both.

The three amide groups whose exchange rates yield the largest stability values are Ala10, Leu11, and Ser90; the values are 8.56, 9.04, and 8.67 kcal/mol, respectively, with an average of 8.8 kcal/mol. These groups are located near the disulfide bond in the 3/10 helix and C-terminal β strand. These structural elements contain several nonpolar side chains (Leu8, Ala10, Leu11, Leu91, and Ile92) that form part of the main hydrophobic core of RNase Sa; the corresponding nonpolar residues in RNase T1, α-sarcin, and barnase form more isolated hydrophobic nuclei (data not shown). Exchange is also slowed but somewhat less for protons forming hydrogen bonds in the α-helix and the strands of the central β-sheet, and the free energy for the unfolding reaction that permits exchange, ΔG_{HX}, is about 7.5 kcal/mol. Glu14, Thr16, and Asp17 on the solvent-exposed face in the first turn of the α-helix and Asp25 at its C terminus are less stable compared to the center of this element of secondary structure.

Table 1: Hydrogen Exchange Rates (h^{-1}) in RNase Sa at 30 °C

residue	k_{rc} at pH* 5.5	0.25 M NaCl	D_2O at pH* 5.5	D_2O at pH* 6	D_2O at pH* 7	0.25 M GdmCl	0.50 M GdmCl	0.75 M GdmCl	1.00 M GdmCl
Asp 1	nd[a]	nd	nd	nd	nd	nd	nd	nd	nd
Val 2	214	>2.5[b]	>2	>2.6	>1.9	>2.6	>2.8	>1.9	>1.7
Ser 3	2750	>2.5	>2	>2.6	>1.9	>2.6	>2.8	>1.9	>1.7
Gly 4	6020	>2.5	>2	>2.6	>1.9	>2.6	>2.8	>1.9	>1.7
Thr 5	2040	>2.5	>2	>2.6	>1.9	>2.6	>2.8	>1.9	>1.7
Val 6	513	0.00236	0.0060	<0.03	0.114	0.00789	0.0245	0.0183	0.035
Cys 7	4166	>2.5	>2	>2.6	>1.9	>2.6	>2.8	>1.9	>1.7
Leu 8	1230	$<4 \times 10^{-4}$ [c]	0.0024	<0.03	≈0.03	0.00109	0.00364	0.0032	0.016
Ser 9	2340	0.043	0.076	0.124	nd	0.225	0.46	0.279	>1.7
Ala 10	3230	0.0018	0.00217	<0.03	0.0665	0.0028	0.00890	0.00617	>1.7
Leu 11	426	$<4 \times 10^{-4}$	0.00013	<0.03	<0.014	0.00050	≈0.0005	≈0.0004	0.0037
Pro 12	nd	nd	nd	nd	nd	nd	nd	nd	nd
Pro 13	nd	nd	nd	nd	nd	nd	nd	nd	nd
Glu 14	288	0.370	1.00	>2.6	>1.9	1.08	1.30	1.25	2.0
Ala 15	1150	0.0044	0.0060	<0.03	0.124	0.0055	0.0152	0.0165	>5
Thr 16	1380	0.122	0.156	0.293	>1.9	0.49	0.830	0.55	0.5
Asp 17	1290	0.170	0.312	0.390	>1.9	0.44	0.61	0.44	0.6
Thr 18	911	0.00105	0.00369	<0.03	0.079	0.0024	0.0080	0.0085	>1.7
Leu 19	676	$<4 \times 10^{-4}$	0.0029	<0.03	0.044	0.00050	0.0030	0.0020	0.013
Asn 20	3090	0.0077	0.0138	0.027	0.28	0.0379	0.0745	0.0464	0.089
Leu 21	891	0.0011	0.00059	<0.03	0.0519	0.00105	0.0046	0.00492	0.020
Ile 22	186	$<4 \times 10^{-4}$	0.00183	<0.03	<0.014	0.00064	0.0022	0.00204	0.011
Ala 23	954	0.30	0.375	0.700	>1.9	1.45	2.2	1.42	>1.7
Ser 24	3800	0.107	0.144	0.266	>1.9	0.427	0.74	0.52	>1.7
Asp 25	1620	1.6	2.1	>2.6	>1.9	>2.6	>2.8	>1.9	>1.7
Gly 26	1990	0.056	0.112	0.115	0.27	0.24	0.30	0.231	>1.7
Pro 27	nd	nd	nd	nd	nd	nd	nd	nd	nd
Phe 28	3710	>2.5	>2	>2.6	>1.9	>2.6	>2.8	>1.9	>1.7
Pro 29	nd	nd	nd	nd	nd	nd	nd	nd	nd
Tyr 30	501	0.068	0.287	0.46	>1.9	0.283	0.47	0.33	>1.7
Ser 31	4260	>2.5	>2	>2.6	>1.9	>2.6	>2.8	>1.9	>1.7
Gln 32	3710	>2.5	>2	>2.6	>1.9	0.065	>2.8	>1.9	>1.7
Asp 33	1290	0.060	0.172	0.245	>1.9	0.275	0.43	0.42	>1.7
Gly 34	1990	0.014	0.041	0.061	nd	>2.6	0.165	0.121	>1.7
Val 35	478	0.0061	0.0195	nd	0.20	0.0221	0.058	0.0377	>1.7
Val 36	234	0.62	1.4	2.2	nd	1.351	>2.8	>1.9	>1.7
Phe 37	676	0.00094	0.00182	<0.03	<0.014	0.00166	0.0047	0.0037	0.022
Gln 38	2140	>2.5	>2	>2.6	>1.9	>2.6	>2.8	>1.9	>1.7
Asn 39	7940	>2.5	>2	>2.6	>1.9	>2.6	>2.8	>1.9	>1.7
Arg 40	4070	>2.5	>2	>2.6	>1.9	>2.6	>2.8	>1.9	>1.7
Glu 41	831	>2.5	>2	>2.6	>1.9	>2.6	>2.8	>1.9	>1.7
Ser 42	2690	≈2.4	>2	>2.6	>1.9	>2.6	>2.8	>1.9	>1.7
Val 43	645	0.61	1.4	2.20	>1.9	1.06	2.1	1.57	>1.7
Leu 44	309	0.026	0.086	0.15	nd	0.087	0.0147	0.065	>1.7
Pro 45	nd	nd	nd	nd	nd	nd	nd	nd	nd
Thr 46	794	>2.5	>2	>2.6	>1.9	>2.6	>2.8	>1.9	>1.7
Gln 47	2949	>2.5	>2	>2.6	>1.9	>2.6	>2.8	>1.9	>1.7
Ser 48	6020	>2.5	>2	>2.6	>1.9	>2.6	>2.8	>1.9	>1.7
Tyr 49	1740	>2.5	>2	>2.6	>1.9	>2.6	>2.8	>1.9	>1.7
Gly 50	3386	>2.5	>2	>2.6	>1.9	>2.6	>2.8	>1.9	>1.7
Tyr 51	1287	0.047	0.127	0.196	nd	0.175	0.297	0.175	0.37
Tyr 52	977	0.75	≈2.3	>2.6	>1.9	≈2.2	1.9	1.27	>1.7
His 53	11 500	0.0037	0.0156	<0.03	0.136	0.0122	0.043	0.040	0.12
Glu 54	3386	0.0025	0.0094	<0.03	0.099	0.0059	0.025	>1.9	>1.7
Tyr 55	616	0.0007	0.0039	<0.03	0.072	0.00193	0.00675	0.00786	>1.7
Thr 56	1548	0.023	0.081	0.097	0.31	0.0973	0.182	0.127	0.18
Val 57	513	0.00201	0.0043	<0.03	0.0718	0.0028	0.00734	0.0046	>1.7
Ile 58	219	0.0135	0.0334	0.059	0.38	0.0787	0.175	0.10	>1.7
Thr 59	812	0.285	1.29	>2.6	>1.9	1.51	1.75	1.08	>1.7
Pro 60	nd	nd	nd	nd	nd	nd	nd	nd	nd
Gly 61	5010	>2.5	>2	>2.6	>1.9	>2.6	>2.8	>1.9	>1.7
Ala 62	933	>2.5	>2	>2.6	>1.9	>2.6	>2.8	>1.9	>1.7
Arg 63	2880	>2.5	>2	>2.6	>1.9	>2.6	>2.8	>1.9	>1.7
Thr 64	1380	>2.5	>2	>2.6	>1.9	>2.6	>2.8	>1.9	>1.7
Arg 65	3230	>2.5	>2	>2.6	>1.9	>2.6	>2.8	>1.9	>1.7
Gly 66	4780	>2.5	>2	>2.6	>1.9	>2.6	>2.8	>1.9	>1.7
Thr 67	2290	>2.5	>2	>2.6	>1.9	>2.6	>2.8	>1.9	>1.7
Arg 68	2880	1.1	>2	>2.6	>1.9	1.87	>2.8	1.3	>1.7
Arg 69	3090	>2.5	0.0080	<0.03	0.098	>2.6	>2.8	>1.9	>1.7
Ile 70	501	0.0025	0.0026	<0.03	<0.014	0.0011	0.0043	0.0024	>1.7
Ile 71	501	$<4 \times 10^{-4}$	0.00195	<0.03	0.069	0.00050	0.0036	0.0020	0.015
Thr 72	810	0.00137	0.0051	<0.03	0.068	0.0025	0.0080	0.0078	>1.7

Table 1 (Continued)

residue	k_{rc} at pH* 5.5	0.25 M NaCl	D_2O at pH* 5.5	D_2O at pH* 6	D_2O at pH* 7	0.25 M GdmCl	0.50 M GdmCl	0.75 M GdmCl	1.00 M GdmCl
Gly 73	1780	0.0054	0.0101	<0.03	0.12	0.0159	0.047	0.0287	>1.7
Glu 74	794	>2.5	>2	>2.6	>1.9	>2.6	>2.8	>1.9	>1.7
Ala 75	2400	>2.5	>2	>2.6	>1.9	>2.6	1.7	>1.9	>1.7
Thr 76	977	>2.5	>2	>2.6	>1.9	>2.6	>2.8	>1.9	>1.7
Gln 77	1860	>2.5	>2	>2.6	>1.9	>2.6	>2.8	>1.9	>1.7
Gln 78	794	1.0	0.78	1.28	>1.9	4.0	>2.8	>1.9	>1.7
Asp 79	1290	0.22	0.22	0.32	>1.9	0.80	1.33	0.95	>1.7
Tyr 80	616	$<4 \times 10^{-4}$	0.0015	<0.04	0.048	0.00067	0.0037	0.0017	>1.7
Tyr 81	575	$<4 \times 10^{-4}$	0.0024	<0.04	0.059	0.00113	0.0043	0.00425	>1.7
Thr 82	1550	0.0016	0.0067	<0.04	≈0.1	0.0031	0.0102	0.00116	0.052
Gly 83	3390	>2.5	>2	>2.6	>1.9	>2.6	>2.8	>1.9	0.27
Asp 84	1290	>2.5	>2	>2.6	>1.9	>2.6	>2.8	>1.9	>1.7
His 85	15 100	>2.5	>2	>2.6	>1.9	>2.6	>2.8	0.0235	>1.7
Tyr 86	575	>2.5	>2	>2.6	>1.9	>2.6	>2.8	>1.9	>1.7
Ala 87	11 000	>2.5	>2	>2.6	>1.9	>2.6	>2.8	>1.9	>1.7
Thr 88	1550	1.1	≈2.7	>2.6	>1.9	>2.6	≈2.8	≈2.1	>1.7
Phe 89	932	>2.5	>2	>2.6	>1.9	>2.6	>2.8	0.0391	>1.7
Ser 90	6020	0.0011	0.0034	<0.03	0.097	0.0027	0.0099	0.010	>1.7
Leu 91	489	0.144	0.199	0.384	>1.9	0.815	1.9	1.3	>1.7
Ile 92	850	$<4 \times 10^{-4}$	0.0035	<0.03	<0.014	0.00050	0.0010	0.0010	0.0063
Asp 93	501	$<4 \times 10^{-4}$	0.0020	<0.03	<0.014	0.00050	0.0015	0.0010	0.010
Gln 94	1150	>2.5	>2	>2.6	>1.9	>2.6	>2.8	>1.9	>1.7
Thr 95	911	1.7	1.3	1.97	>1.9	>2.6	>2.8	0.64	>1.7
Cyr 96	9110	0.020	0.0527	0.070	0.373	0.0686	0.161	0.095	>1.7

[a] nd = not determined. [b] Lower rate limit; less than half of the original signal remained after the deadtime. Lower rate limit = 0.693/experimental deadtime given in column 3 of Supplementary Table 1 in the Supporting Information. [c] Upper rate limit; more than half of the originial signal remained at the end of the experiment. Upper rate limit = 0.693/duration of the experiment given in column 6 of Supplementary Table 1 in the Supporting Information.

Significant but weaker protection against hydrogen exchange was found for the amide groups of residues donating hydrogen bonds in turns (Tyr30 and Asp33) or to side-chain groups (Glu14, Tyr30, Val43, Leu44, Thr56, and Thr95). The amide groups of Val43 and Leu44, which donate hydrogen bonds to the side-chain carbonyl of Asn39, have ΔG_{HX} values of 3.7 and 5.0 kcal/mol, respectively. The side-chain amide group of Asn39, which is hydrogen-bonded to the backbone carbonyl group of Leu44, also shows moderate protection, with $k_{obs} = 1.0\ h^{-1}$. The importance of these interactions to the stability and rigidity of the loop has been established previously (*6*). In contrast, none of the amide groups in the loop formed by residues 60−67 is measurably protected against exchange. The amide groups of Ser8, Glu14, Tyr30, Thr56, Thr88, and Thr95 form hydrogen bonds to charged carboxylate groups and show moderate protection from exchange.

Hydrogen Exchange and Chemical Denaturation Yield Similar Stability Values for RNase Sa. The conformational stability of RNase Sa, as determined by GdmCl denaturation at 30 °C as monitored by CD spectroscopy (Figure 4), was found to be 6.7 ± 0.4 kcal/mol in H_2O and slightly more stable, 7.5 ± 0.2 kcal/mol, in D_2O. The dependence of ΔG on the GdmCl concentration, the *m* value, is very similar in H_2O (2.30 ± 0.13 kcal mol^{-1} M^{-1}) and D_2O (2.32 ± 0.20 kcal mol^{-1} M^{-1}). As described above, the correction for the Xaa−Pro cis/trans isomerization for RNase Sa is 1.60 kcal/mol (*26*, *29*, *36*, *37*). Upon taking into account the contribution of proline isomerization, the values for the conformational stability obtained by hydrogen exchange (8.8 ± 0.3 kcal/mol) and GdmCl denaturation (7.5 ± 0.2 + 1.6 kcal/mol = 9.1 ± 0.2 kcal/mol) are found to be similar. Considering that the 50 mM NaAc buffer present in the latter experiment increased the stability by 0.2 kcal/mol (see below), these values are practically identical.

Sodium Chloride Stabilizes RNase Sa Against Thermal Denaturation. To characterize the effect of NaCl on RNase Sa stability, thermal denaturation experiments were performed in different concentations of this salt and the results are shown in Figure 5A. Denaturation was followed by CD at 234 nm, which is sensitive to the environment of chiral aromatic groups, which are chiefly found in the central β-sheet. Low concentrations of NaAc or NaCl have small effects on the conformational stability, suggesting that there is not a tight, specific binding site for their ions on the protein. Higher concentrations of NaCl do stabilize the protein. After 0.25 M NaCl, the protein is about 1.0 kcal mol^{-1} more stable than in water. Above 0.25 M NaCl, the conformational stability continues to increase but with a smaller slope (Figure 5A, also see ref *10*).

Low Concentrations of GdmCl Stabilize RNase Sa. Thermal denaturation experiments were also measured in GdmCl, a chaotropic salt. Concentrated aqueous solutions of GdmCl effectively solvate all of the various chemical moieties of proteins, leading to their unfolding (*38*, *39*). Although high concentrations of GdmCl (>3 M) unfold RNase Sa, it can be expected to stabilize RNase Sa at lower concentrations because it is a salt. The results (Figure 5B) show that RNase Sa is indeed stabilized at low concentrations of GdmCl; at 0.25 M GdmCl, the enzyme is about 0.5 kcal mol^{-1} more stable. At higher concentrations, the denaturant effect becomes dominant, and at 0.75 M GdmCl, the stability is less than in water. The stabilizing effect of GdmCl appears to be saturated by 0.25 M GdmCl, because, at this concentration and above, the dependence of ΔG on the GdmCl concentration (the *m* value) becomes approximately equal

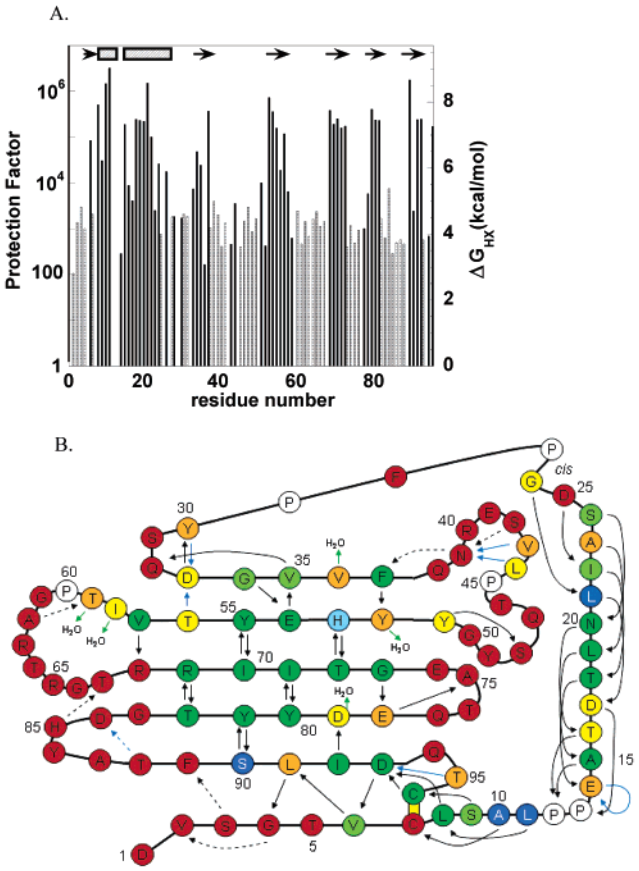

FIGURE 3: Conformational free energy of RNase Sa measured by hydrogen exchange. (A) Protection factors (left *y* axis) and ΔG_{HX} (right *y* axis) for RNase Sa amide groups in D_2O at pH* 5.5 and 30 °C. Striped bars represent upper limits for fast exchanging groups, and filled bars show experimentally measured values. The approximate positions of secondary structural elements (helices as hashed rectangles, β strands as arrows) are indicated. (B) Hydrogen-bonding network and ΔG_{HX} values in RNase Sa. Color code: dark blue, $\Delta G_{HX} > 8.5$ kcal mol^{-1}; light blue, $8.5 < \Delta G_{HX} > 7.8$ kcal mol^{-1}; dark green, $7.8 < \Delta G_{HX} > 7.0$ kcal mol^{-1}; light green, $7.0 < \Delta G_{HX} > 6.0$ kcal mol^{-1}; yellow, $6.0 < \Delta G_{HX} > 5.0$ kcal mol^{-1}; orange, $\Delta G_{HX} < 5.0$ kcal mol^{-1} but measurable; red, exchange faster than 2 h^{-1}. Proline residues are shown in white, and every fifth residue is numbered. Hydrogen bonds, NH → acceptor are shown in black arrows when the acceptor group is in the main chain, in blue arrows when the acceptor group is in a side chain, and in green arrows when the acceptor group is a structural water molecule. Broken line arrows indicate H-bonds affording no measurable protection. The Cys7−Cys96 disulfide bond is shown as a thick yellow line. Please note that because of the twisting of the β-sheet, the position of the loops relative to the α-helix in this two-dimensional drawing is different from that of the actual tertiary structure (see Figure 1).

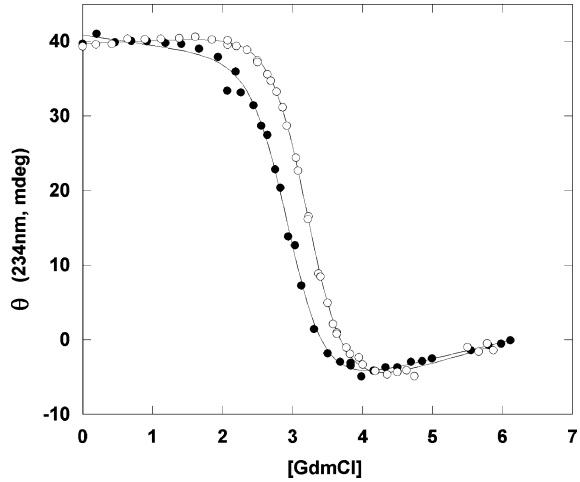

FIGURE 4: Equilibrium unfolding of RNase Sa in H_2O (●) or D_2O (○). The lines represent the fit of a nonlinear least-squares equation to the data. Conditions, 30 °C and pH 5.9 or pH* 5.5, respectively.

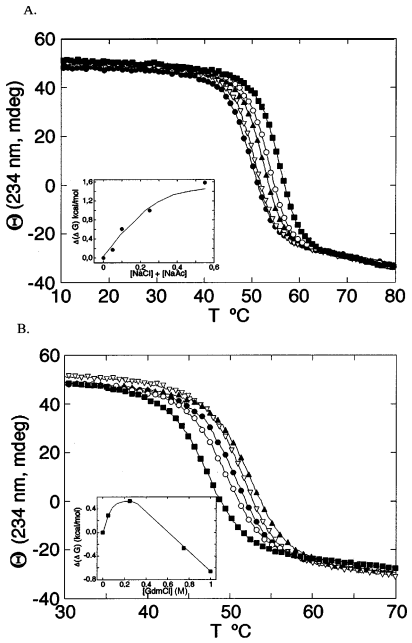

FIGURE 5: Salt effects on the stability of RNase Sa against thermal denaturation. (A) Thermal denaturation curves of RNase Sa various concentrations of NaCl: No salt or sodium acetate, ●; 50 mM sodium acetate, no NaCl, ▽; 50 mM NaAc and 50 mM NaCl, ▲; 50 mM NaAc and 200 mM NaCl, ○; 50 mM NaAc and 500 mM NaCl, ■. (B) Thermal denaturation curves of RNase Sa in various concentrations of GdmCl: 0 mM GdmCl, ●; 50 mM GdmCl, ▽; 250 mM GdmCl, ▲; 750 mM GdmCl, ○; 1000 mM GdmCl, ■. All contained 50 mM NaAc as a buffer. Insets in both A and B show the change in RNase Sa stability with changing salt concentrations. The lines drawn in the insets are to guide the eye.

to that measured in equilibrium denaturation experiments (2.30 kcal mol^{-1} M^{-1}).

NaCl (0.25 M) Slows RNase Sa Hydrogen Exchange. The hydrogen exchange rate constants for RNase Sa measured in 0.25 M NaCl are, on average, about half as large as those measured in the absence of added salt (Table 1); however, the decrease in the rate of exchange induced by salt is not uniform throughout the protein. The exchange rates of amide groups in and near β strands show larger decreases. Equations 4 and 5 and the exchange rates with and without NaCl were used to calculate the residue-level changes in the conformational stability induced by salt, and the results are shown Figure 6A. The largest stability increases were observed for Tyr55 and Thr59, 1.0 and 0.91 kcal/mol, respectively, and are close to the value of the global stabilization determined by thermal denaturation monitored by CD. Smaller stability changes, averaging about 0.3 kcal/mol, were seen in the 3/10 and α helices. The 3/10 and α helices are significantly more solvent-exposed (average 19%) than the central β-sheet (average 5%). It is also interesting that helices are richer in negatively charged residues than the β-sheet.

Stabilization of the Central β Sheet of RNase Sa by 0.25 M GdmCl. The exchange rate constants measured in D_2O can be compared with those determined in 0.25 M GdmCl

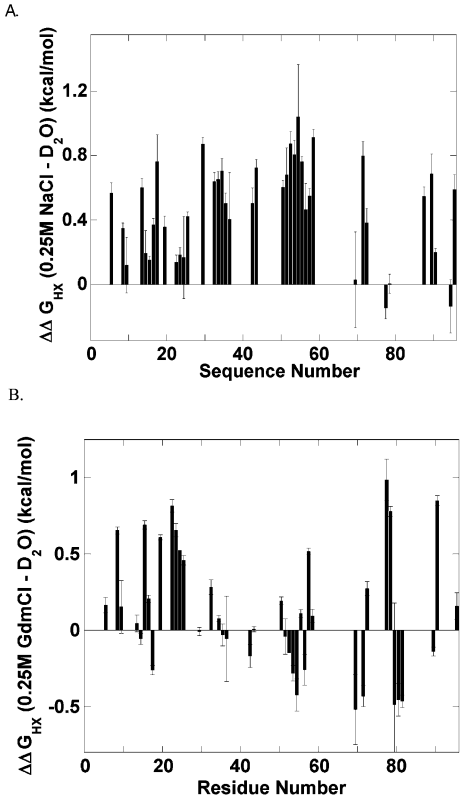

FIGURE 6: Salt effects on local stability in RNase Sa measured by hydrogen exchange. (A) Changes in ΔG_{HX} induced by 0.25 M NaCl. (B) Changes in ΔG_{HX} caused by the presence of 0.25 M GdmCl. The errors bars shown are the square root of the sum of the square of the errors for ΔG_{HX} (salt) and ΔG_{HX} (D_2O) (A) or ΔG_{HX} (GdmCl) and ΔG_{HX} (D_2O) (B).

(Table 1), which was observed to stabilize RNase Sa by 0.5 kcal/mol against thermal denaturation (see above). This low concentration of GdmCl slowed the exchange and stabilized several amide groups of the central β-sheet (Tyr55, Ile70, Thr72, Tyr80, Tyr81, and Thr82), and the magnitude of the stabilization was about the same as detected by thermal denaturation (Figure 6B). In contrast, the exchange rates of the amide groups of residues Ser9 and Ala10 in the 3/10 helix reveal that this element of secondary structure is destabilized by about 0.15 kcal/mol, and the α-helix and residues Val58, Glu78, Asp79, and Leu91 show greater destabilization.

Exchange in 0.50, 0.75, and 1.00 M GdmCl. To characterize the unfolding events that permit hydrogen exchange at specific sites in RNase Sa, hydrogen exchange measurements were performed in 0.50, 0.75, and 1.00 M GdmCl. As the GdmCl concentration is increased, the observed exchange rate constants increase (Table 1) and the ΔG_{HX} values for the slowest exchanging residues decrease from almost 8 kcal mol^{-1} at 0.50 M GdmCl to about 7 kcal mol^{-1} in 1.00 M GdmCl (Figure 7A). At all three GdmCl concentrations, the slowest exchanging NH groups are concentrated in the 3/10 helix or C-terminal β strand, with NH groups in the central β-sheet and α-helix, showing slightly lower stabilities. For some amide groups in turns and loops, exchange becomes too fast to follow at high GdmCl concentrations.

The dependence of the conformation free energy on the GdmCl concentration ($\delta\Delta G_i/\delta$[GdmCl]) is termed the m_i value and is roughly proportional to the amount of surface area exposed in the opening reaction or partial unfolding event that exposes the particular hydrogen-bonded NH "*i*" to permit exchange. These values have been used to characterize subglobal unfolding events that open the structure to permit exchange (*18*, *19*, *40*). Here, we cannot determine m_i values at very low GdmCl concentrations but only above 0.25 M GdmCl where the electrostatic interactions are reasonably well-screened. Overall, there is a strong linear correlation between the magnitude of the m_i and $\Delta G_{HX(i)}$ values ($R = 0.89$, $n = 48$); therefore, the larger the partial unfolding transition, the greater the energy needed to provoke it. Because of the reduced number of GdmCl concentrations studied here, the uncertainty in the m_i values is high (±30% or more; *41*); therefore, the m_i values given here should be interpreted with caution. Nevertheless, when the m_i values are grouped into broad categories to permit a qualitative interpretation, as shown in Figure 7B, and when the m_i values of residues belonging to the same structural motif are considered together, a general overview of the unfolding events permitting hydrogen exchange in RNase Sa can be obtained. The exchange of amide groups forming isolated hydrogen bonds in turns, at the edges of β-sheets, or in the first four residues and C cap of the α-helix occurs during local unfolding events in which less than a quarter of the protein structure unfolds (Figure 7B, colored red and yellow). Most of the amide groups in the α-helix and main β-sheet (green) exchange through an intermediate state that is mostly unfolded. Eight residues (blue) have m_i values close to the global *m* value measured by equilibrium denaturation (2300 cal mol^{-1} M^{-1}), which indicates that there is restriction to the complete unfolding of RNase Sa. Two of these residues, Phe37 and Glu54, are in the central β-sheet; two more, Leu21 and Ile22, are in last turn of the α-helix; and the remaining four, Leu8, Leu11, Ile92, and Asp93, are close to the disulfide bond, in the 3/10 helix or C-terminal β strand.

DISCUSSION

Low Protection Against Hydrogen Exchange Correlates with Dynamic Motion in RNase Sa. The low level of protection against exchange in the loops, such as the one formed by residues 60−67, is consistent with their significant dynamic behavior (*17*). Amide groups near the disulfide bond, which acts to restrict the dynamic motion of the backbone, show slowed exchange. Disulfide bonds also appear to stabilize zones of exchange-resistant structure in ribonuclease A (*42*). Proline residues also impose restrictions on the flexibility of the polypeptide chain in both the native and denatured states. The rigidity imposed by Pro12 and Pro13 may account in part for the slow exchange of preceding amide groups in the 3/10 helix. The carbonyl groups of these residues also accept hydrogen bonds from the amide groups in the first turn of the helix, protecting them from exchange.

Hydrogen Bonding to Water Molecules and Charged Side Chains. Although most of the amide groups showing slowed exchange participate in networks of hydrogen bonds in secondary structural elements, some have formed hydrogen bonds with water molecules or side-chain groups. In regard to the amide groups hydrogen-bonded to water molecules, it should be noted that their exchange rates do not reflect the occupancy time of the bound water molecules, which

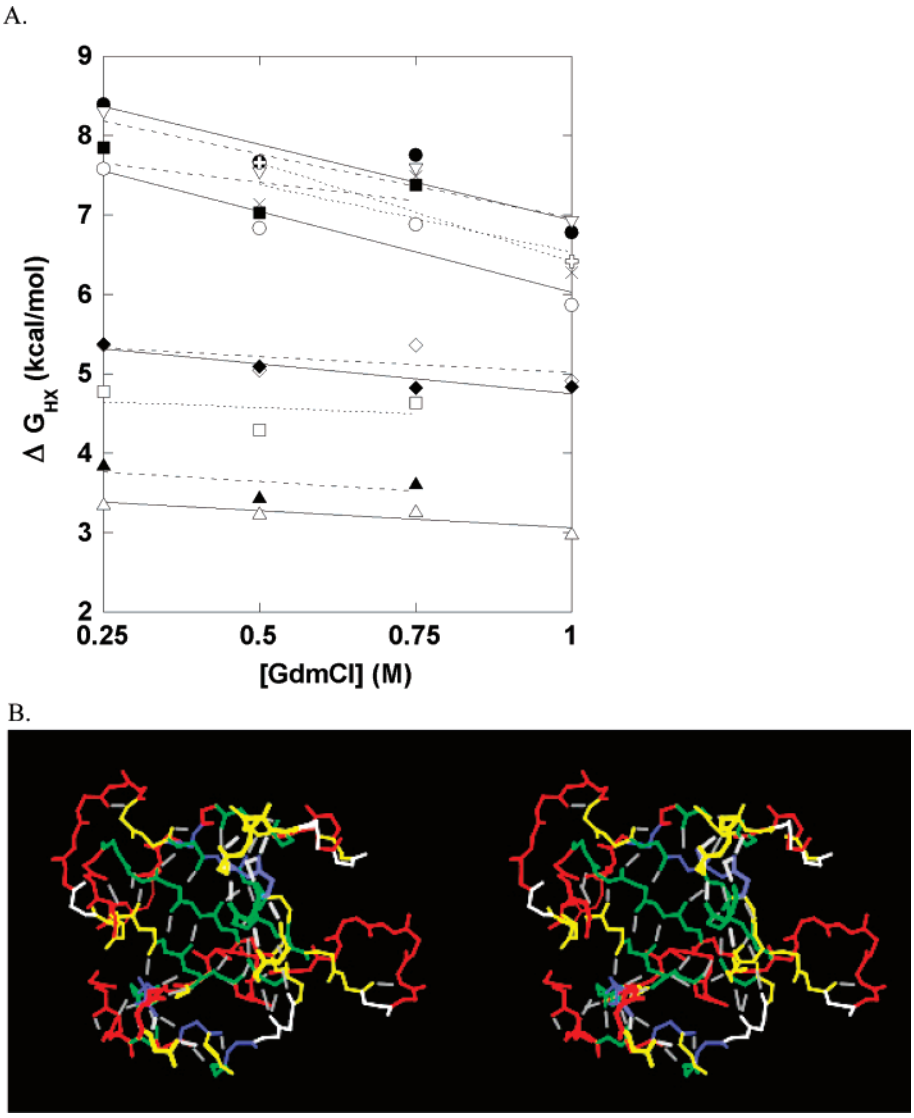

FIGURE 7: Local unfolding events mapped by m_i values in RNase Sa in D_2O at pH* 5.5 and 30 °C representative m_i values. (A) Values of ΔG_{HX} versus [GdmCl] over the concentration range of 0.25 to 1.00 M and lines depicting the fit of a least-squares linear equation to these data are shown. The slope of these lines is the m_i value. Leu8 (3/10 helix) ●, —; Glu14 (α-helix) △, —; Ile22 (α-helix) ○, —; Asp33 (turn) ◆, —; Val43 (turn) ▲, - - -; Tyr51 (preceding a β strand) ◇, - - -; His53 (β strand) ▽, - - -; Ile58 (coil) □, •••; Ile70 (β stand) ■, - - -; Ile71 (β strand) ×, •••; Asp93 (C-terminal β strand) open cross, •••. (B) Local unfolding events mapped by m_i values in RNase Sa in D_2O at pH* 55 and 30 °C. Cross-eyed stereoview of RNase Sa. Main-chain atoms are colored according to their m_i values: exchange too rapid to measure, red; m_i < 500 cal mol^{-1} M^{-1} but measurable, yellow; 500 < m_i < 1800 cal mol^{-1} M^{-1}, green; and m_i > 1800 cal mol^{-1} M^{-1}, blue. Proline residues are shown in white, and main-chain hydrogen bonds are shown in gray.

have been observed to be less than 10 ms in other proteins (*43*), but are determined by the occurrence of local unfolding events. The hydrogen bonds donated by the amide protons of Ser8, Thr56, Thr88, and Thr95 to charged carboxylate acceptors appear to be strong, as evidenced by their significantly (>0.5 ppm) downfield-shifted chemical-shift values (*2*, *44*) and by the depressed p*K* values of their acceptor groups (*8*).

RNase Sa Conformational Stability. At pH* 5.5 and 30 °C, the exchange mechanism for RNase Sa is found to be EXII. Exchange from other proteins has been generally found to follow the EXII mechanism at similar conditions of acidic pH and where the protein stability is high. Here, we find equivalent values for the conformational stability of RNase Sa using hydrogen exchange and GdmCl denaturation monitored by CD spectroscopy, once the stabilizing effect of D_2O and the contribution of the proline isomerization were taken into account. Similar stability values from hydrogen exchange and thermal or chemical denaturation have been observed for other proteins (*26*), consistent with the idea that the exchange behavior of the slowest exchanging protons occurs from a globally unfolded state that is thermodynamically equivalent to the heat or denaturant-induced unfolded state. Our present results with RNase Sa provide further support for those conclusions.

Salts can affect protein stability in a number of ways: (i) Tight binding to a particular site in the folded or unfolded protein will increase the stability of the bound state. This effect could be important even at low concentrations of salt and will depend on the identity and valence of the ion. (ii) Moderate (a few tenths molar) concentrations of dissolved ions can affect protein stability by screening electrostatic interactions of groups present in the native or denatured state of the protein. This effect will depend on the concentration and valence of the ions. A recent, meticulous thermodynamic study of thioredioxin has revealed intriguing evidence

suggesting that GdmCl more effectively screens charge−charge interactions than NaCl (*45*). (iii) Higher concentrations of dissolved salts can indirectly affect protein stability by altering the water structure. This latter phenomena, known as the Hofmeister effect (*46*, *47*), can be broken down into two major components: (iiia) dissolved ions increase the surface tension of water, making solvation of the nonpolar components more difficult but also (iiib) interact favorably with peptide groups, increasing their solvation. Hofmeister effects depend on both the identity of the ion and its concentration. For NaCl, the salting-out action on the nonpolar groups (iiia) balances out its salting-in action on the peptide groups (iiib), and therefore the overall Hofmeister effect on protein stability exerted by NaCl is small. In contrast, GdmCl strongly interacts with peptide groups (*38*, *39*) and is a potent protein denaturant.

Here, the effect of two salts, NaCl and GdmCl, on RNase Sa stability has been measured both by global denaturation methods and by hydrogen exchange. No striking stability increase was detected at low concentrations by either salt; this is evidence against the existence of a tight binding site for monovalent ions in RNase Sa. Moderate concentrations of NaCl were previously observed to globally stabilize RNase Sa, and this observation lead to the conclusion that salt acts by screening unfavorable electrostatic interactions in the native state or favorable electrostatic interactions in the denatured state or both (*10*). From hydrogen exchange, we can examine the effect only on the native state, because unfolded states are rarely populated.

The hydrogen exchange results obtained in either 0.25 M NaCl or 0.25 M GdmCl reveal a lower stabilization than was detected by thermal denaturation. We believe that further work, including experimental work following exchange from model peptides in different salts at various concentrations and computational simulations of the interaction of salt ions with proteins, is needed to fully understand the results reported here. Part of this difference is probably due to the fact that only the rates of residues exchanging from a globally unfolded state are expected to experience the full stabilization by salt. The per-residue variation in stability upon adding salt seems to reflect some contribution from the Hofmeister effect, because the most stabilized amide groups belong to residues in the central β-sheet, deep in the protein core, whose neighboring hydrophobic moieties are being "salted-out", and more superficial NH groups are less stabilized by NaCl, as if their peptide groups were being "salted-in".

The results may also reflect a direct effect of salt on hydrogen exchange. Model compound studies show that negative charges in proteins repel the DO^- ion, decreasing the amide exchange rate, whereas positive charges attract DO^-, increasing exchange rates (*16*). The addition of salts could screen these effects, leading to increased exchange rates for negatively charged regions of RNase Sa (the helices) and lower exchange rates for positively charged regions (active-site face of the β-sheet, see Figure 1B). This effect is in line with the smaller salt-induced decrease in the exchange rates of the helices relative to the β-sheet (Figure 6) and suggests that regions of high charge density in proteins may affect hydrogen exchange beyond the consecutive side-chain effects meticulously characterized by Englander and co-workers (*16*), which are included in the ΔG_{HX} values presented here. In a previous study, the effect of salt on hydrogen exchange in bovine pancreatic trypsin inhibitor was found to correlate with the local charge density (*48*).

Mechanism of RNase Sa Unfolding. Higher concentrations of GdmCl provoke increasingly rapid exchange from the amide groups in RNase Sa. Many of the groups that are most sensitive to increasing GdmCl are near the Cys7−Cys96 disulfide bond in the 3/10 helix or C-terminal β strand. This finding suggests that these elements of secondary structure and their hydrophobic core might be the last to unfold upon RNase Sa denaturation and might be the first in oxidized RNase Sa to refold. The N- and C-terminal regions of cytochrome *c* also exchange only upon global unfolding, and further experiments show that they form first during refolding (*49*). However, the results with RNase Sa are surprising, considering that in previously characterized ribonucleases, the residues showing the most resistance to exchange were localized in the center of the main β-sheet. The different result obtained here might reflect the fact that the hydrophobic groups in the 3/10 helix and last β strand of RNase Sa are more fully integrated into the hydrophobic core than the corresponding residues in RNase T1, α-sarcin, and barnase. The idea that homologous proteins might have different unfolding and refolding pathways is not so surprising considering the insightful results of Udgaonkar and co-workers (*50*), who were able to alter the unfolding pathway of a small protein by making only single-residue substitutions, and the theoretical expectations of funnel models for protein folding, which predict multiple pathways with slight differences in energy (*51*).

Conclusions. Here, we have studied the conformational stability of RNase Sa using hydrogen exchange monitored by NMR. NaCl and low concentrations of GdmCl stabilize RNase Sa, but the magnitude of the stabilization detected by HX is less than that observed in thermal unfolding experiments and appears to correlate with positive charge density and burial. The most protected amide proton groups lie not only in the central β-sheet, as occurs in other ribonucleases, but also in the C-terminal edge β strand and the 3/10 helix, which lie near the Cys6−Cys96 disulfide bond and suggests that this bond plays an important role in stabilizing the local structure. Both hydrogen exchange and equilibrium unfolding experiments yield identical values for the conformational stability, 9.0 kcal/mol at 30 °C and pH * 5.5.

ACKNOWLEDGMENT

We are grateful to David Schell for making ^{15}N-RNase Sa and Dr. José Luis Neira for insightful discussions. The constructive criticism of two anonymous referees is sincerely appreciated. We thank Prof. Jorge Santoro for support.

SUPPORTING INFORMATION AVAILABLE

Summary of NMR-monitored exchange measurements (Supplementary Table 1). This material is available free of charge via the Internet at http://pubs.acs.org.

REFERENCES

1. Ševčík, J., Dauter, Z., Lamzin, V. S., and Wilson, K. S. (1996) Ribonuclease from *Streptomyces aureofaciens* at atomic resolution, *Acta Crystallogr., Sect. D 52*, 327−344.

2. Laurents, D. V., Peréz-Cañadillas, J. M., Santoro, J., Schell, D., Hebert, E. J., Pace, C. N., Bruix, M., and Rico, M. (1999) Sequential assignment and solution secondary structure of doubly labelled ribonuclease Sa, *J. Biomol. NMR, 14*, 89−90.
3. Pace, C. N., Heinemann, U., Hahn, U., and Saenger, W. (1991) Ribonuclease T1: Structure, function, and stability, *Angew. Chem. Int. Ed. Engl. 30*, 343−360.
4. Bycroft, M., Ludvigsen, S., Fersht, A. R., and Poulsen, F. M. (1991) Determination of the three-dimensional solution structure of barnase using nuclear magnetic resonance spectroscopy, *Biochemistry 30*, 8697−8701.
5. Pérez-Cañadillas, J. M., Campos-Olivas, R., Santoro, J., Lacadena, J., Martínez del Pozo, Á., Gavilanes, J. G., Rico, M., and Bruix, M. (2000) Solution structure of the cytotoxic ribonuclease α-sarcin, *J. Mol. Biol. 299*, 1061−1073.
6. Hebert, E. J., Giletto, A., Ševčík, J., Urbanikova, L., Wilson, K. S., Dauter, Z., and Pace, C. N. (1998) Contribution of a conserved asparagine to the conformation stability of ribonucleases Sa, Ba, and T1, *Biochemistry 37*, 16192−16200.
7. Shaw, K. L., Grimsley, G. R., Yakovlev, G. I., Markarov, A., and Pace, C N. (2001) The effect of net charge on the solubility, activity, and stability of ribonuclease Sa, *Protein Sci. 10*, 1206−1215.
8. Laurents, D. V., Huyghues-Despointes, B. M. P., Bruix, M., Thurlkill, R. L., Schell, D., Newsom, S., Grimsley, G. R., Shaw, K. L., Treviño, S., Rico, M., Briggs, J. M., Antosiewicz, J. M., Scholtz, J. M., and Pace, C. N. (2003) Charge−charge interactions are key determinants of the p*K* values of ionizable groups in ribonuclease Sa (pI = 3.5) and a basic variant (pI = 10.2), *J. Mol. Biol. 325*, 1077−1092.
9. Huyghues-Despointes, B. M. P., Thurlkill, R. L., Daily, M. D., Schell, D., Briggs, J. M., Antosiewicz, J. M., Pace, C. N., and Scholtz, J. M. (2003) p*K* values of histidine residues in ribonuclease Sa: Effect of salt and net charges, *J. Mol. Biol. 325*, 1093−1105.
10. Pace, C. N., Alston, R. W., and Shaw, K. L. (2000) Charge−charge interactions influence the denatured state ensemble and contribute to protein stability, *Protein Sci. 9*, 1395−1398.
11. Pace, C. N., Hebert, E. J., Shaw, K. L., Schell, D., Both, V., Krajcikova, D., Ševčík, J., Wilson, K. S., Duter, Z., Hartley, R. W., and Grimsley, G. (1998) Conformational stability and thermodynamics of folding of ribonucleases Sa, Sa2, and Sa3, *J. Mol. Biol. 279*, 271−286.
12. Grimsley, G. R., Shaw, K., and Pace, C. N. (1999) Increasing protein stability by altering long-range Coulombic interactions, *Protein Sci. 8*, 1843−1849.
13. Pradeep, L., and Udgaonkar, J. B. (2004) Effect of salt on the urea unolded form of barstar probed by *m*-value measurements, *Biochemistry 43*, 11393−11402.
14. Huyghues-Despointes, B. M. P., Pace, C. N., Englander, S. W., and Scholtz, J. M. (2001) Measuring the conformation stability of a protein by hydrogen exchange, in *Methods in Molecular Biology*, Vol. 168, Protein Structure, Stability, and Folding, pp 69−92 (Murphy, K. P., Ed.) Humana Press, Inc., Totwa, NJ.
15. Molday, R. S., Englander, S. W., and Kallen, R. G. (1972) Primary structure effects on peptide group hydrogen exchange, *Biochemistry 11*, 150−158.
16. Bai, Y., Milne, J. S., Mayne, L., and Englander, S. W. (1993) Primary structure effects on peptide group hydrogen exchange, *Proteins 17*, 75−86.
17. Laurents, D. V., Pérez-Cañadillas, J. M., Santoro, J., Rico, M., Schell, D., Pace, C. N., and Bruix, M. (2001) Solution structure and dynamics of ribonuclease Sa, *Proteins 44*, 200−211.
18. Mayo, S. L., and Baldwin, R. L. (1993) Guanidinium chloride induction of partial unfolding in amide proton exchange in RNase A, *Science 269*, 192−197.
19. Bai, Y., Sosnick, T. R., Mayne, L.; Englander S. W. (1995) Protein folding intermediates: Native-state hydrogen exchange, *Science 269*, 192−197.
20. Hebert, E. J., Grimsley, G. R., Hartley, R. W., Horn, G., Schell, D., Garcia, S., Both, V., Ševčík J., and Pace, C. N. (1997) Purification of ribonucleases Sa, Sa2, and Sa3 after expression in *Escherichia coli*, *Protein Expression Purif. 11*, 162−168.
21. Hvidt, A., and Nielsen, S. O. (1996) Hydrogen exchange in proteins, *Adv. Protein Chem. 21*, 287−386.
22. Arrington, C. B., and Robertson, A. D. (1997) Microsecond protein folding kinetics from native state hydrogen exchange, *Biochemistry 35*, 8686−8691.
23. Myers, J. K., Pace, C. N., and Scholtz, J. M. (1995) Denaturant *m*-values and heat capacity change relation to changes in accessible surface area of protein unfolding, *Protein Sci. 4*, 2138−2148.
24. Loftus, D., Gbenle, G. O., Kim, P. S., and Baldwin, R. L. (1986) Effects of denaturants on amide proton exchange rates: A test for structure in protein fragments and folding intermediates, *Biochemistry 25*, 1428−1431.
25. Bodenhausen, G., and Ruben, D. J. (1980) Natural abundance nitrogen-15 NMR by enhanced heteronuclear spectrosopy, *Chem. Phys. Lett. 69*, 185−189.
26. Huyghues-Despointes, B. M. P., Scholtz, J. M., and Pace, C. N. (1999) Protein conformational stabilities can be determined from hydrogen exchange rates. *Nat. Struct. Biol. 6*, 910−912.
27. Santoro, M. M., and Bolen, D. W. (1988) Unfolding free energy changes determined by the linear exprapolation method: 1. Unfolding of phenylmethanesulfonyl α-chymotrypsin using different denaturants, *Biochemistry 27*, 8063−8068.
28. Pace, C. N., Shirley, B. A., and Thomson, J. A. (1989). Measuring the conformational stablity of a protein, *Protein Structure: A Practical Approach*, p 316, IRL Press, New York.
29. Reimer, U., Scherer, G., Drwello, M., Kruber, S., Schutkowski, M., and Fischer G. (1998) Side-chain effects of peptidyl-prolyl cis/trans isomerisation, *J. Mol. Biol. 279*, 449−460.
30. Becktel, W. J., and Schellman, J. A. (1987) Protein stability curves. *Biopolymers 26*, 1859−1877.
31. Ševčík, J., Lamzin, V. S., Dauter, Z., and Wilson, K. S. (2002) Atomic resolution data reveal flexibility in the structure of RNase Sa, *Acta Crystallogr., Sect. D 58*, 1307−1313.
32. Koradi, R., Billeter, M., and Wüthrich, K. (1996) MOLMOL: A program for display and analysis of macromolecular structures, *J. Mol. Graphics 14*, 51−55.
33. Martínez-Oyanedel, J., Heinemann, U., and Saenger, W. (1991) Ribonuclease T1 with free recognition and catalytic site: Crystal structure analysis at 1.5 Å resolution, *J. Mol. Biol. 222*, 335−352.
34. Mauguen, Y., Hartley, R. W., Dodson, E. J., Dodson, G. G., Bricogne, G., Chothia, C., and Jack, A. (1982) Molecular structure of a new family of ribonucleases, *Nature 297*, 162−164.
35. Skelton, N. J., Kördel, J., Akke M., and Chazin, W. J. (1992) Nuclear magnetic resonance studies of the internal dynamics in apo, (Cd^{2+}), and (Ca^{2+}) calbindin D9k, *J. Mol. Biol. 227*, 1100−1117.
36. Kiefhaber, T., Kohler, H., and Schmid, F. X. (1992) Kinetic coupling between protein folding and prolyl isomerization I. Theoretical models, *J. Mol. Biol. 224*, 217−229.
37. Kiefhaber, T., and Schmid, F. X. (1992) Kinetic coupling between protein folding and prolyl isomerization: II. Folding of ribonuclease A and ribonuclease T1, *J. Mol. Biol. 224*, 231−240.
38. Tanford, C. (1970) Protein denaturation: Part C: Theoretical models for the mechanism of denaturation, *Adv. Protein Chem. 24*, 1−95.
39. Nandi, P. K., and Robinson, D. R. (1984) Effects of urea and guanidine hydrochloride on peptide and nonpolar groups, *Biochemistry 23*, 6661−6668.
40. Chamberlain, A. K., Handel, T. M., and Marqusee, S. (1996) Detection of rare partially folded molecules in equilibrium with the native conformation of RNase H, *Nat. Struct. Biol. 3*, 782−787.
41. Sachs, L. (1982). *Applied Statistics: A Handbook of Techniques*. Springer, New York.
42. Neira, J. L., Sevilla, P., Menéndez, M., Bruix, M., and Rico, M. (1999) Hydrogen exchange in ribonuclease A and ribonuclease S: Evidence for residual structure in the unfolding state under native conditions, *J. Mol. Biol. 285*, 627−643.
43. Otting, G., Liepinsh, E., and Wüthrich, K. (1991) Protein hydration in aqueous solution, *Science 254*, 974−980.
44. Bundi, A., and Wüthrich, K (1979) Use of amide conformational shifts for studies of polypeptide conformation, *Biopolymers 18*, 299−311.
45. Pérez-Jiménez, R., Godoy-Ruiz, R., Ibarra-Molero, B., and Sánchez-Ruiz, J. M. (2004) The efficiency of different salts to screen charge interactions in proteins: A Hofmeister effect? *Biophys. J. 86*, 2414−2429.
46. Hofmeister, F. (1888) Zur Lehre von der Wirkung der Salze. Zweite Mittheilung, *Arch. Exp. Pathol. Pharmakol. 24*, 247−260.
47. Baldwin, R. L. (1996) How Hofmeister ion interactions affect protein stability, *Biophys. J. 71*, 2056−2063.

48. Christoffersen, M., Bolvig, S., and Tüchsen, E. (1996) Salt effects on the amide hydrogen exchange of bovine pancreatic trypsin inhibitor, *Biochemistry 35*, 2309−2315.
49. Maity, H., Maity, M., Krishna, M. M. G., Mayne, L., and Englander, S. W. (2005) Protein folding: The stepwise assembly of foldon units, *Proc. Natl. Acad. Sci. U.S.A. 102*, 4741−4746.
50. Zaidi, F. N., Nath, U., and Udgaonkar, J. B. (1997) Multiple intermediates and transition states during protein unfolding, *Nat. Struct. Biol. 4*, 1016−1024.
51. Wolynes, P. G., Onuchic, J. N., Thirumalai, D. (1995) Navigating the folding routes, *Science 267*, 1619−1620.

BI050142B